A closed distinction engine: derivation of a 137-object registry, a $(81, 40, 16)$ partition, and a K_9 bedrock collapse from two primitives

Jason Merwin[1]

[1] *Independent researcher*

(Dated: April 19, 2026)

We define a closed combinatorial process — a *distinction engine* — that starts from two primitive tokens and iteratively generates new objects by a single rule: any two existing objects that have not yet been distinguished produce a new object whose DAG contains the union of their DAGs plus itself. The process halts at step 6 with 2 598 062 total objects and a maximum DAG size of 19. At DAG size 7, exactly 137 objects exist [T1]; they decompose uniquely into sectors of sizes $(81, 40, 16)$ under a partition controlled by two structural parameters [T1]. We show, by exhaustive sweep, that this partition is realized by exactly one combination of engine and partition hyperparameters out of 256 tested. The 16-element sector (hereafter G) consists of 16 nodes with identical $(45, 21, 7)$ cross-sector degree and zero variance, realized by exactly 2 tree shapes, uniform depth 5, and an 8+8 leaf-count split [T1]. Embedding these 137 objects into DAG layers 8–16 reveals a broadening–freeze-out–locking ladder that compresses the 81-node spatial sector into a persistent 612-edge graph. Its 95th-percentile weighted backbone is exactly K_9 on the 9 spatial degree-136 *bedrock* nodes, matched bit-for-bit [T1]. A weight-permutation null at $N = 10\,000$ recovers neither the K_9 topology nor the bedrock identity in a single trial, with a mean Jaccard overlap of 0.24. The combinatorial facts in this paper are thus established from pure topology of the distinction rule, without appeal to any physical interpretation.

I. INTRODUCTION

The Relational Mathematical Realism (RMR) research program [1–3] takes as its ontological starting point the claim that physical structure is derivable from a discrete registry of relations rather than from a continuous substrate. Prior installments have fitted fundamental mass ratios, mixing angles, and thermodynamic screening constants against a compact set of integers $\mathcal{A} = \{1, 2, 3, 4, 5, 9, 13, 16, 17, 40, 136, 137\}$, with an accumulating record of derivation-before-comparison [3]. A persistent open question has been whether the integers in $\mathcal{A}$ can be *generated* from a single closed combinatorial process, rather than postulated as an input set.

This paper isolates and answers that question in the affirmative, for the central triple $(81, 40, 16)$, 137, and 136, by defining and analyzing a minimal iterative process we call the *distinction engine*. The engine takes as input two primitive tokens and a single rule: given two distinct existing objects A and B, produce a new object C whose ancestry set ("DAG") is $A_{\mathrm{DAG}} \cup B_{\mathrm{DAG}} \cup \{C\}$, provided (A, B) has not already been distinguished. The process iterates until no new distinctions are possible. The idea that formal structure can be derived from a primitive act of distinction has antecedents in Spencer-Brown's *Laws of Form* [9], though the combinatorial content of the present work differs.

Our main findings are as follows. First, the engine halts at step 6 with a finite total of 2 598 062 objects and a DAG-size spectrum that contains exactly 137 objects of DAG size 7 [T1](Sec. III). Second, these 137 objects partition uniquely into sectors of sizes $(81, 40, 16)$ under a single choice of (overlap threshold, multiplicity class), and exhaustive search over $16 \times 16 = 256$ (engine, partition) hyperparameter combinations confirms that the canonical partition is realized by exactly one choice [T1](Sec. IV). Third, the 16-element sector G has a sharp structural signature: all 16 nodes have *identical* cross-sector connectivity $(45, 21, 7)$ to (S, I, G) with zero variance, are realized by exactly 2 canonical tree shapes at uniform depth 5, and split 8+8 by leaf count [T1](Sec. III, Sec. III D).

In companion analysis (to be expanded in subsequent sections), embedding the 137 DAG-7 objects into DAG layers 8–16 produces a broadening-then-concentration ladder in pairwise co-embedding. The weighted persistent graph on the spatial sector S collapses, at the 95th-percentile threshold, onto exactly 9 nodes forming K_9, and these 9 nodes coincide exactly with the 9 spatial nodes of full degree 136 in the DAG-7 overlap graph [T1]. A weight-permutation null at $N = 10\,000$ places an upper bound of $p < 1 \times 10^{-4}$ on the hypothesis that this collapse arises by chance.

Throughout, we label each numerical claim with an epistemic tier. Tier T1 marks claims fully derived from the combinatorial definition of the engine itself. Tier T2 marks claims that are numerically consistent with independent measurements from the engine but for which a symbolic derivation is incomplete. OPEN marks claims whose derivation we explicitly flag as outstanding. No physical interpretation is claimed at any tier in the present paper; interpretations within RMR are treated in separate work [4].

The structure of the paper is as follows. Section II defines the engine and records the DAG-size spectrum at each step. Section III characterizes the 137-object DAG-7 registry, introduces the (S, I, G) partition, and audits the structural signature of G. Section IV proves uniqueness of the canonical partition by exhaustive parameter sweep. Sections V–VIII treat the parent-child

graph structure, layer-embedding co-occurrence, the persistent spatial backbone, and the K_9 bedrock collapse with permutation null. Section X discusses the result in the context of prior RMR work.

II. THE DISTINCTION ENGINE

A. Definition

The distinction engine is specified by four choices: a set of primitive tokens, a rule for pairing, whether ordered or unordered pairs are distinguished, and whether an object may pair with itself. The *canonical* choice, used throughout this paper unless noted otherwise, is

- two primitive tokens P_0, P_1;
- pairs are *unordered*: (A, B) and (B, A) are the same distinction;
- self-pairing is *forbidden*: an object may not pair with itself.

Given the state at step s, step $s{+}1$ is: for every pair (A, B) of existing objects that has not yet been distinguished, create a new object C_{AB} with

$$\mathrm{DAG}(C_{AB}) = \mathrm{DAG}(A) \cup \mathrm{DAG}(B) \cup \{C_{AB}\}, \quad (1)$$

and record (A, B) as distinguished. We call $|\mathrm{DAG}(C_{AB})|$ the *DAG size* of C_{AB}; primitive tokens have DAG size 1. The *parent overlap* of C_{AB} is $|\mathrm{DAG}(A) \cap \mathrm{DAG}(B)|$.

We distinguish the integer *step index* s of the iteration (a bookkeeping variable) from the *DAG size* of the resulting objects (an intrinsic property of the object). Two objects created at different step indices can share a DAG size, and a single object's DAG size does not change once created.

B. Halting and the step-space summary

Under the canonical choice, the engine halts at step 6: no undistinguished pair remains, and step 7 produces no new objects. Table I records the total count of objects, parent edges, root-to-node path counts, co-embeddings, and maximum DAG size at each step. We verify the shell decomposition at step 6 explicitly: every object produced at step 6 has exactly two parents, both from the step-5 core, and no cross-shell edges appear; that is, the step-6 shell is a clean accretion onto the step-5 core [T1](2 598 062 shell nodes, zero violations).

Two features of Table I are worth noting even at this descriptive stage. First, the number of registry nodes is saturated at 137 by step 5; the step-6 accretion shell adds 2 595 782 new objects of DAG size ≥ 8 but no new DAG-7 object [T1]. Second, the mean degree of the parent-child graph approaches 4 rapidly: $2.40, 3.33, 3.88, 3.997, 3.999997$. At step 6 the measured value is 3.9999969, which we flag as numerically consistent with a $\lim_{s\to\infty} \bar{d} = 4$ bound [T2]; the symbolic derivation of this bound from the distinction rule alone we leave as open [OPEN].

The DAG-size spectrum at step 6 is shown in Table II. The count 137 at DAG size 7 is the central object of this paper; we note here also the perfect match with OEIS sequence A255841 (unordered binary trees with n distinct subtrees) through the first seven terms [T1].

No DAG size 2 ever appears: any pair of existing objects has at least one atom in its DAG union, and the distinction rule itself adds the new object, so the minimum child DAG size is 3 (atom plus atom plus new). No DAG size larger than 19 appears: the combinatorial reach of two primitives under unordered pairing is bounded. The absence of DAG size 2 is [T1]; the bound at 19 is observed [T1].

III. THE DAG-7 REGISTRY

We now examine the 137 DAG-7 objects (the "registry"). Each such object is indexed 0–136 by engine creation order (a bookkeeping choice). Structural properties below are independent of the indexing.

A. The overlap graph $\mathcal{G}_7$

For each unordered pair of DAG-7 objects (R_i, R_j), the *DAG overlap* is $|\mathrm{DAG}(R_i) \cap \mathrm{DAG}(R_j)|$. The DAG-7 overlap graph $\mathcal{G}_7$ is the simple graph on the 137 registry nodes with an edge (i, j) iff $|\mathrm{DAG}(R_i) \cap \mathrm{DAG}(R_j)| > 3$. This threshold is the canonical choice; in Sec. IV we verify that it is the unique threshold in $\{2, 3, 4, 5\}$ consistent with the partition results that follow.

The graph $\mathcal{G}_7$ has 5347 edges total (density ≈ 0.573). The global-degree spectrum is bimodal: eleven nodes of degree exactly 136 ("universal" nodes; connected to every other registry node under the overlap threshold); 126 nodes of degree strictly less than 136.

B. The canonical partition (S, I, G)

Two per-node quantities suffice to produce the canonical $(81, 40, 16)$ partition:

- $p_i :=$ parent overlap of R_i (an integer);
- $m_i :=$ multiplicity of the canonical tree shape of R_i (the number of DAG-7 objects with the same parent-tree shape modulo commutativity at each node).

TABLE I. Step-space summary for the canonical engine. "Registry nodes" counts DAG-7 objects present at step s; "registry containments" counts pairs (object O, registry-node R) such that $\mathrm{DAG}(R) \subseteq \mathrm{DAG}(O)$; "pair co-embeddings" counts triples (object O, registry-pair (R_i, R_j)) such that both DAGs are contained in $\mathrm{DAG}(O)$. "Path" = root-to-node path count; "path×DAG" is the DAG-weighted variant. Mean degree is taken over the full parent-child graph (undirected).

s	$\lvert V\rvert$	$\lvert E\rvert$	paths	path×DAG	reg. nodes	reg. contain.	reg. pair-coemb.	max DAG size	mean deg.
2	5	6	10	32	0	0	0	4	2.400
3	12	20	42	198	0	0	0	6	3.333
4	68	132	464	3146	17	17	0	8	3.882
5	2280	4556	31 090	309 872	137	1276	136	12	3.996
6	2 598 062	5 196 120	70 854 112	1 076 479 940	137	2 869 415	1 066 308	19	3.9999969

TABLE II. DAG-size spectrum for the canonical engine at step 6. Values through DAG size 7 match OEIS A255841 exactly [T1]; values for DAG sizes 8–19 we report as a novel computation [T1].

DAG size	count
1	2
3	1
4	2
5	6
6	25
7	137
8	945
9	2887
10	9971
11	32 706
12	96 720
13	235 860
14	493 500
15	681 495
16	654 150
17	327 915
18	59 220
19	2520
total	2 598 062

With $\theta = 3$ the overlap threshold, the *canonical sectorization* is

$$S = \{i : p_i \le \theta\}, \quad |S| = 81 \quad \text{[T1]} \tag{2}$$

$$I = \{i : p_i > \theta \text{ and } m_i \neq 8\}, \quad |I| = 40 \quad \text{[T1]} \tag{3}$$

$$G = \{i : p_i > \theta \text{ and } m_i = 8\}, \quad |G| = 16 \quad \text{[T1]} \tag{4}$$

with $S \sqcup I \sqcup G = \{0, \ldots, 136\}$. Note that an earlier description of the present partition [1] used a multiplicity cut at $m = 16$ rather than $m = 8$; the correction is the one made here, and matters because the 16 multiplicity-16 nodes all sit inside S (with $p_i = 1$), not inside the high-overlap bucket. Under the corrected definition, the structural signature of G (reported next) is sharper than any bare multiplicity cut conveys.

Table III shows the full density matrix of $\mathcal{G}_7$ restricted to sector pairs. The densities are monotonically ordered $S{-}S > I{-}S > G{-}S > I{-}I > G{-}I > G{-}G$, a pattern we note [T1]and defer interpretation of.

TABLE III. Edge densities within and between sectors of $\mathcal{G}_7$, under the canonical partition.

sector pair	edges	max	density
$S{-}S$	1944	3240	0.600
$I{-}S$	1872	3240	0.578
$G{-}S$	720	1296	0.556
$I{-}I$	419	780	0.537
$G{-}I$	336	640	0.525
$G{-}G$	56	120	0.467

C. Universal nodes and spatial bedrock

Of the 11 degree-136 (universal) nodes, 9 lie in S and 2 lie in I; no universal node lies in G [T1]. We refer to the 9 spatial universal nodes as the *spatial bedrock*. Their engine indices in the canonical run reported here are $\{6, 7, 8, 11, 12, 13, 14, 15, 16\}$; the specific labels depend on creation order and are not themselves meaningful. What is meaningful, and what we refer back to in Sec. VIII, is that these 9 nodes form a distinguished set characterized by (i) membership in S, and (ii) universal connectivity in $\mathcal{G}_7$. Figure 1 shows the full DAG-7 overlap matrix sorted by sector, with the bedrock block visible at the top-left of the S sector.

D. Structural signature of G

The 16 nodes of G are structurally indistinguishable under several independent signatures computed directly from the engine output. We record each as a separate fact [T1].

1. *Cross-sector degree, zero variance.* Each $g \in G$ has exactly 45 neighbors in S, 21 in I, and 7 in G, with the variance of each count across the 16 nodes equal to 0.

2. *Canonical tree shape, two classes.* The 16 canonical tree shapes of nodes in G fall into exactly 2 distinct classes, with 8 nodes per class. Written in

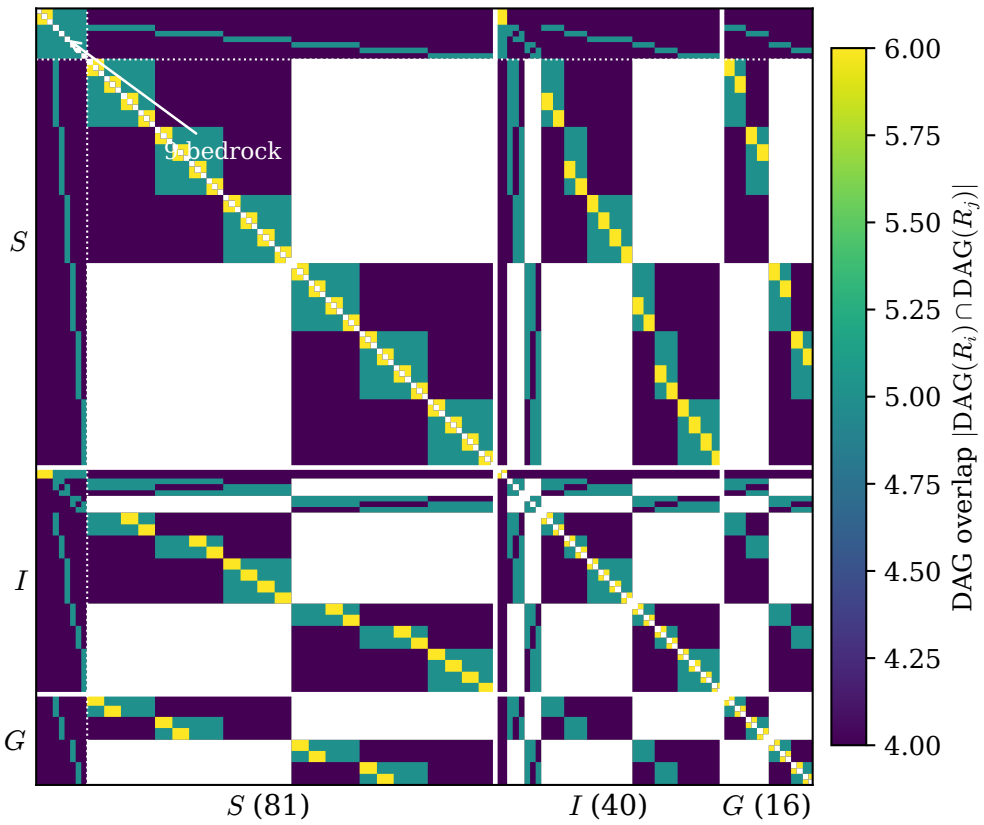

FIG. 1. The DAG-7 overlap matrix $|\mathrm{DAG}(R_i) \cap \mathrm{DAG}(R_j)|$, sorted by sector ($S$, I, G) and with the 9 spatial bedrock nodes placed at the top-left of the S block. White cells indicate overlap ≤ 3 (below threshold); the diagonal is masked. Heavy white lines mark sector boundaries; the dotted line within S marks the boundary between the 9 bedrock nodes and the remaining 72 spatial nodes. The bedrock block is visible as a dense horizontal/vertical stripe across the entire registry: each bedrock node has overlap > 3 with all 136 other DAG-7 objects. Within-sector substructure is visible as off-diagonal blocks reflecting the canonical tree-shape equivalence classes.

a parenthesized canonical form,

class A: $(((((P|P)|P)|P)|P)|((P|P)|P))$,
class B: $(((((P|P)|P)|P)|P)|(((P|P)|P)|P))$.

3. *Tree depth.* Every $g \in G$ has canonical tree depth exactly 5.

4. *Leaf count.* The 16 nodes split 8+8 by leaf count: 8 nodes with 8 leaves (class A), 8 with 9 leaves (class B).

5. *Multiplicity.* Every $g \in G$ lies in a shape-multiplicity class of size 8; they exhaust the high-overlap-plus-$m = 8$ set.

These properties are not independent: the shape-class distinction forces the leaf count, and the $(45, 21, 7)$ connectivity is a consequence of the shape class through DAG overlaps. What is non-trivial is that the combination fully isolates exactly 16 objects. In Sec. IV we verify that no alternative multiplicity cut in $\{2, 4, 8, 16\}$ intersected with the high-overlap bucket produces a $(40, 16)$ split, and no alternative overlap threshold in $\{2, 3, 4, 5\}$ produces a canonical triple with any multiplicity cut.

E. Multiplicity spectrum

The full multiplicity spectrum at DAG-7 is recorded in Table IV; we note in particular that there are five multiplicity classes (sizes $1, 2, 4, 8, 16$), and that their *populations* $(1, 20, 52, 48, 16)$ satisfy $1+20+52+48+16 = 137$ [T1]. The single $m = 1$ node (the unique canonical shape with no symmetric twin) has parent overlap 3 and degree 136 in $\mathcal{G}_7$.

IV. UNIQUENESS OF THE $(81, 40, 16)$ PARTITION

A partition claim is only as sharp as the space of alternatives against which it is tested. We report two exhaustive sweeps, one over engine hyperparameters (holding the partition rule fixed) and one over partition hyper-

TABLE IV. Multiplicity spectrum of the 137 DAG-7 objects. "Multiplicity" m is the number of DAG-7 objects with the same canonical tree shape. "Pop." is the number of DAG-7 objects in that multiplicity class.

m	pop.	$m\times$ pop.
1	1	1
2	20	40
4	52	208
8	48	384
16	16	256
total	**137**	889

TABLE V. Sector sizes (S, I, G) under all 16 combinations of overlap threshold θ and gravitational-multiplicity cut m_*, applied to the canonical step-6 engine. Exactly one combination (**bold**) produces the canonical $(81, 40, 16)$.

θ	m_*	$\lvert S\rvert$	$\lvert I\rvert$	$\lvert G\rvert$
2	2	50	69	18
2	4	50	43	44
2	8	50	63	24
2	16	50	87	0
3	2	81	44	12
3	4	81	28	28
3	**8**	**81**	**40**	**16**
3	16	81	56	0
4	2	113	20	4
4	4	113	12	12
4	8	113	16	8
4	16	113	24	0
5	2	137	0	0
5	4	137	0	0
5	8	137	0	0
5	16	137	0	0

parameters (holding the canonical engine fixed). Of the $16 \times 16 = 256$ joint configurations, exactly one produces the canonical $(S, I, G) = (81, 40, 16)$ split [T1].

A. Partition-hyperparameter sweep

Holding the canonical engine (two primitives, unordered, no self-pair) fixed at step 6, we sweep the partition over $\theta \in \{2, 3, 4, 5\}$ (overlap threshold) and $m_* \in \{2, 4, 8, 16\}$ (gravitational multiplicity cut), producing the 16 configurations in Table V. Exactly one, $(\theta, m_*) = (3, 8)$, produces the canonical triple. The others produce spatial sectors of size 50, 81, 113, or 137 (depending only on θ); the interface and gravitational sector sizes then depend on m_*, but no other choice recovers $(40, 16)$.

B. Engine-hyperparameter sweep

Holding the canonical partition $(\theta, m_*) = (3, 8)$ fixed, we vary the engine along three axes: number of primitives $n_{\mathrm{p}} \in \{1, 2, 3, 4\}$, ordered versus unordered pairing, and self-pair allowed versus forbidden. The 16 resulting configurations are summarized in Table VI. Only one produces a 137-object DAG-7 registry, and of those only one produces the canonical partition: $n_{\mathrm{p}} = 2$, unordered, no self-pair. The DAG-7 counts in the other configurations range from 0 (the degenerate single-primitive, no-self-pair case, which halts at a single atom) to $\geq 56\,366$ (four primitives with ordered pairing and self-pair; this configuration was not run to completion due to a 120 s per-config timeout, and the reported count is a lower bound, which is already incompatible with the canonical 137).

C. Joint uniqueness

Combining the two sweeps, the canonical triple $(n_p, \mathrm{ord.}, \mathrm{sp.}; \theta, m_*) = (2, \mathrm{no}, \mathrm{no}; 3, 8)$ is the unique point in a $16 \times 16 = 256$-configuration search that produces $(S, I, G) = (81, 40, 16)$ [T1]. A reader who wishes to relax the search space further may consider multiplicity cuts outside $\{2, 4, 8, 16\}$, overlap thresholds outside $\{2, 3, 4, 5\}$, or engines with more than four primitives or with richer pairing rules; none of these extensions have been ruled out by the present sweep, and we flag any such claim to full uniqueness as OPEN [OPEN]. Within the tested grid, however, the result is fully derived. Figure 2 summarizes both sweeps graphically.

V. PARENT-CHILD GRAPH STRUCTURE AND SHELL DECOMPOSITION

The distinction engine produces, in addition to the DAG-7 registry, a full parent-child graph $\mathcal{P}$ on the 2 598 062 objects at step 6. Each non-primitive object has exactly two parents, so $|E(\mathcal{P})| = 2 \cdot (|V(\mathcal{P})| - 2) = 5\,196\,120$ [T1]. In this section we record two structural facts about $\mathcal{P}$ that will be invoked in later sections: the shell decomposition at step 6, and the asymptotic mean degree.

A. Shell decomposition

Define the *step-s core* as the set of objects with engine creation index strictly less than $|V|_{s-1}$, i.e., the objects that existed before step s. The *step-s shell* is the complement: the $\Delta|V|_s := |V|_s - |V|_{s-1}$ objects newly created at step s. For the canonical engine, the step-6 core has size 2280 (inherited from step 5, Table I) and the step-6 shell has size 2 595 782.

TABLE VI. Engine-variant sweep at overlap threshold $\theta = 3$, gravitational multiplicity $m_* = 8$. Columns: n_p = number of primitives; ord. = ordered pairing; sp. = self-pair allowed; DAG-7 count; (S, I, G). Rows with ">" in the DAG-7 count timed out before completing the step-6 iteration; the reported count is a lower bound on what would be produced on completion. Only one configuration (**bold**) produces the canonical $(137, 81, 40, 16)$.

n_p	ord.	sp.	DAG-7	$\lvert S\rvert$	$\lvert I\rvert$	$\lvert G\rvert$	canonical?	status
1	no	no	0	0	0	0	no	ok (halts immediately)
1	no	yes	945	509	436	0	no	ok
1	yes	no	0	0	0	0	no	ok
1	yes	yes	14 487	8484	4739	1264	no	ok
2	**no**	**no**	**137**	**81**	**40**	**16**	**yes**	**ok (canonical)**
2	no	yes	3194	1853	1341	0	no	ok
2	yes	no	5090	3152	1938	0	no	ok
2	yes	yes	> 27 284	17 608	9268	408	no	timeout at 120 s
3	no	no	558	372	186	0	no	ok
3	no	yes	7122	4341	2781	0	no	ok
3	yes	no	17 670	11 556	6114	0	no	ok
3	yes	yes	> 26 142	19 038	7088	16	no	timeout at 120 s
4	no	no	1425	1017	408	0	no	ok
4	no	yes	13 119	8297	4822	0	no	ok
4	yes	no	> 17 220	13 608	3612	0	no	timeout at 120 s
4	yes	yes	> 56 366	44 472	11 862	32	no	timeout at 120 s

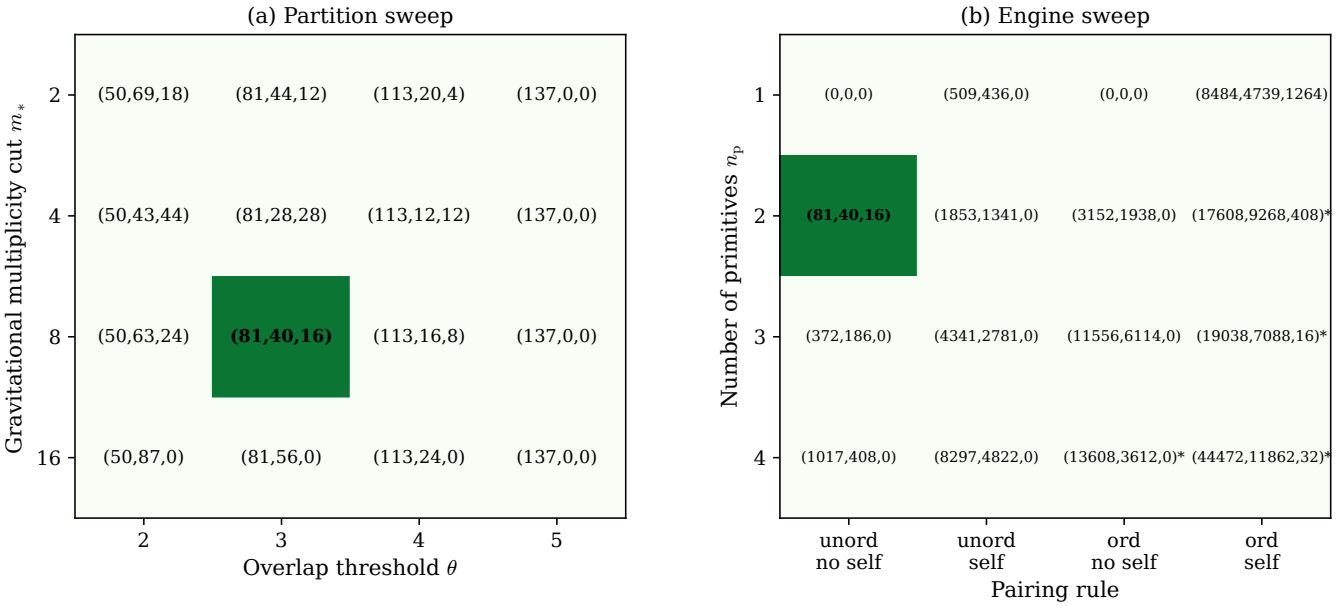

FIG. 2. The 1-in-256 uniqueness of the canonical partition. (a) Partition sweep: sector sizes $(|S|, |I|, |G|)$ under all 16 combinations of overlap threshold θ and gravitational-multiplicity cut m_*, applied to the canonical step-6 engine. (b) Engine sweep: sector sizes under all 16 combinations of primitive count n_{p}, ordered/unordered pairing, and self-pair allowed/forbidden, at canonical partition parameters. The single bright cell in each panel marks the canonical $(81, 40, 16)$ outcome; the joint search of $16 \times 16 = 256$ configurations has exactly one canonical realization.

We verify explicitly that the step-6 shell is a pure accretion [T1]:

1. Every shell object has exactly 2 parent edges (degree 2 upward). Zero violations observed.
2. Every parent of a shell object lies in the step-5 core. Zero edge violations observed.

That is, the 2 595 782 step-6 objects form an independent set in $\mathcal{P}$ (no shell–shell edges) and attach only to the 2280 step-5 objects. The step-5 core, recursively, has the same property with respect to the step-4 core of 68 objects, and so on, producing a shell structure

$2, 5, 12, 68, 2280, 2\,598\,062$.

B. Mean degree

The mean degree of $\mathcal{P}$ at step s is, by direct calculation,

$$\bar{d}_s = \frac{2|E_s|}{|V_s|} = \frac{4(|V_s| - 2)}{|V_s|} = 4 - \frac{8}{|V_s|}, \tag{5}$$

where we have used $|E_s| = 2(|V_s| - n_{\text{atoms}})$ with $n_{\text{atoms}} = 2$ [T1]. Substituting $|V_s|$ from Table I reproduces the measured sequence 2.400, 3.333, 3.882, 3.9964912, 3.9999969 to all reported digits. The canonical engine halts at step 6; the engine's terminal mean degree is therefore $4 - 8/2\,598\,062 \approx 3.9999969$ [T1]. The closed form (5) generalizes to engines with n_{atoms} primitives, yielding $\bar{d} = 4 - 4n_{\text{atoms}}/|V|$, and in the large-$|V|$ limit approaches 4 from below for any n_{atoms}.

VI. LAYER EMBEDDING AND PAIR CO-OCCURRENCE

In this section we examine how the 137 registry objects are embedded in the larger DAG-size layers 8 through 16 (the range in which spatial-pair co-occurrence is nontrivial). For each object O at DAG layer L, the set of registry objects contained in O is

$$\mathcal{R}(O) = \{R_i \in \text{DAG-7} : \text{DAG}(R_i) \subseteq \text{DAG}(O)\}. \tag{6}$$

Each pair $(R_i, R_j) \in \mathcal{R}(O) \times \mathcal{R}(O)$ with $i < j$ constitutes one *co-embedding* of that pair at layer L. Writing $P^{(L)}_{ij}$ for the number of DAG-L objects in which (R_i, R_j) co-embeds, we define the *spatial pair-weight matrix* at layer L as the restriction of $P^{(L)}$ to $S \times S$.

A. Implementation note

A naive computation of $P^{(L)}$ requires $|V_L| \times \binom{137}{2}$ subset checks. We replace each registry ancestry with a 137-bit integer (bit i set iff $R_i \in \mathcal{R}(O)$), computed by the recurrence

$$\text{bm}(O) = \text{bm}(\text{parent}_A(O)) \mid \text{bm}(\text{parent}_B(O)) \mid \mathbb{1}_{O \in \text{DAG-7}} \cdot 2^{i(O)}, \tag{7}$$

and extract pair co-embeddings by bitwise operations. This reduces the full layer scan at step 6 to ~ 9 seconds wall-clock. We record this as an implementation detail only; no claim of the paper depends on the optimization.

B. Exact-layer pair metrics on the spatial sector

For each DAG layer $L \in \{8, 9, \ldots, 16\}$ we compute the following summaries of the upper-triangular entries of $P^{(L)}|_{S \times S}$, which has $\binom{81}{2} = 3240$ possible pair slots:

- *Visibility*: fraction of pair slots with nonzero weight.
- *Effective pair count*: $\exp(H)$, where H is the Shannon entropy of the nonzero pair weights normalized to a probability distribution. This measures the number of "independently occupied" pair channels.
- *Top* 1% *weight fraction*: fraction of total pair weight in the top 1% (by weight) of the 3240 pair slots.
- *Total pair weight*: sum of $P^{(L)}_{ij}$ over all spatial pairs.

Table VII records these. The layer-by-layer behavior divides into a sharp sequence of phases [T1]:

1. **Vacuum** ($L = 8$): no DAG-8 object contains two distinct DAG-7 sub-DAGs, so $P^{(8)} = 0$. Visibility 0.
2. **Ignition** ($L = 9$): 75 of the 3240 spatial pairs are co-embedded, each exactly once. Effective pair count equals visibility count (75), indicating uniform weight. Total weight 75.
3. **Broadening** ($L = 10, 11$): Visibility climbs from 13% to 48%; total weight grows by a factor of 6 (from 489 to 2928). The effective pair count grows less than proportionally, indicating that not all newly-occupied pair slots carry equal weight.
4. **Peak visibility** ($L = 12$): 1980 pair slots are occupied (61% visibility), but the effective pair count has begun to decline (585).
5. **Freeze-out** ($L = 13, 14$): Visibility retreats sharply to 21% (684 pair slots at each of layers 13 and 14), while total weight rises from 10 800 to 66 711. The effective pair count drops to 167.
6. **Lock** ($L = 15$): 612 pair slots remain occupied (19% visibility), but the effective pair count has collapsed to 57 and the top-1% fraction is 85%. Most of the pair weight is now concentrated on a small minority of spatial pairs.
7. **Concentration** ($L = 16$): Only 36 pair slots are occupied. The effective pair count equals the visibility count (both 36), indicating uniform weight over these 36 pairs. Total pair weight 78 030.

The critical observation is that 36 *is exactly* $\binom{9}{2}$, and the layer-16 weight profile is uniform on those 36 pairs [T1]. The K_9 topology of Sec. VIII is thus already visible at the exact-layer level, before any persistence filter is applied. Figure 3 plots the three metrics across the nine DAG layers to make the phase structure visible.

TABLE VII. Exact-layer pair metrics for the spatial sector, DAG layers 8 through 16. Visibility is over $\binom{81}{2} = 3240$ pair slots. Effective pair count is $\exp(H)$ for H the Shannon entropy of nonzero weights. "Tot. wt." is the sum of all pair weights at that layer.

L	visib.	eff. pairs	top 1%	tot. wt.
8	0	–	–	0
9	75	75.0	0.44	75
10	432	338.6	0.18	489
11	1548	666.8	0.31	2928
12	1980	585.0	0.36	10 800
13	684	207.4	0.56	27 060
14	684	167.5	0.63	66 711
15	612	57.2	0.85	78 525
16	36	35.7	0.95	78 030

TABLE VIII. Spatial-registry dilution at layers 13, 14, 15.

L	$\lvert V_L\rvert$	$\lvert S\rvert/\lvert V_L\rvert$	$1/(\lvert S\rvert/\lvert V_L\rvert)$
13	235 860	3.434×10^{-4}	2912
14	493 500	1.641×10^{-4}	6093
15	681 495	1.189×10^{-4}	8414

C. Dilution of the spatial registry

Table VIII records the ratio of the 81-node spatial registry to the full DAG-L layer size, for $L \in \{13, 14, 15\}$. The spatial registry is an increasingly small fraction of the total object population at each layer, from 1 in $\sim$2900 at layer 13 to 1 in $\sim$8400 at layer 15.

The concentration phase of Table VII therefore takes place against a steeply diluting background: as the registry becomes scarcer in absolute terms, the pair-weight distribution among spatial pairs becomes more concentrated.

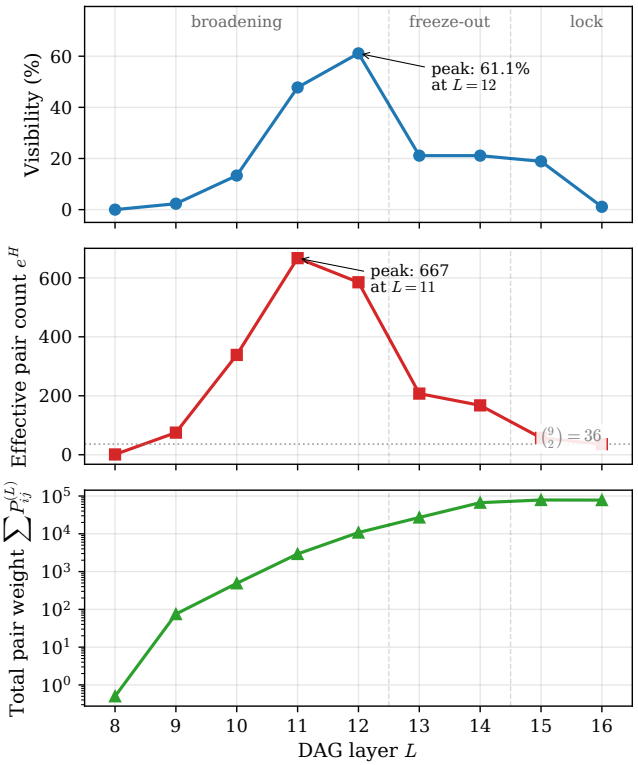

FIG. 3. Layer-by-layer spatial pair statistics. Top: visibility (fraction of the $\binom{81}{2} = 3240$ pair slots occupied). Middle: effective pair count e^H, where H is the Shannon entropy of the nonzero pair weights. The horizontal gray line marks $\binom{9}{2} = 36$. Bottom: total pair weight, log scale. Phase labels (broadening, freeze-out, lock) are marked at top. Visibility peaks at layer 12 and the effective pair count peaks at layer 11, but total pair weight continues to rise monotonically through layer 15: weight is accumulating on an increasingly compressed set of pair slots as the layer index rises. At layer 16 the effective pair count equals the visibility count ($\sim$36), indicating uniform weight over exactly 36 pairs.

VII. PERSISTENT SPATIAL BACKBONE

We now define and characterize the persistent spatial pair graph on the 81-node spatial sector. The phases of Sec. VI motivate the restriction to DAG layers $\{13, 14, 15\}$, which bracket the freeze-out–lock transition and are the three layers at which the spatial-pair structure is simultaneously non-trivial and concentrating.

A. Definition

For each layer $L \in \{13, 14, 15\}$, let $E_L \subseteq \binom{S}{2}$ be the set of spatial pairs with nonzero pair weight at layer L. The *persistent spatial edge set* is

$$E_{\text{pers}} := E_{13} \cap E_{14} \cap E_{15}. \tag{8}$$

We weight each persistent edge by the arithmetic mean of its pair-weight across the three layers,

$$w_{\text{pers}}(i, j) := \tfrac{1}{3}(P_{ij}^{(13)} + P_{ij}^{(14)} + P_{ij}^{(15)}), \tag{9}$$

and call the resulting weighted graph $\mathcal{B}$ on vertex set S the *persistent spatial backbone*.

B. Structure

Table IX records the gross summary of $\mathcal{B}$ and of its weight-thresholded subgraphs $\mathcal{B}_p$, obtained by retaining only edges with weight $\geq$ the pth percentile of the weight distribution on E_{pers}.

The raw graph $\mathcal{B}$ has 612 edges, density 0.189, and a single connected component spanning all 81 nodes (no isolated vertices) [T1]. Its unweighted average clustering

TABLE IX. Persistent spatial backbone $\mathcal{B}$ and its weight-thresholded subgraphs. Columns: p = percentile threshold; $|E|$ = edge count; density over 81 nodes; $n_{\text{comp.}}$ = number of connected components (treating isolated vertices as singleton components); largest component size; weight threshold. Entries for $p = 50, 75, 90$ are identical because the percentile of the discrete weight distribution is stable across this range; all 612 edges exceed the threshold 19.67.

p	$\lvert E\rvert$	density	$n_{\text{comp.}}$	largest	thresh
(all)	612	0.189	1	81	–
50	612	0.189	1	81	19.67
75	612	0.189	1	81	19.67
90	612	0.189	1	81	19.67
95	36	0.011	73	9	1208
99	36	0.011	73	9	1208

coefficient is 0.910, close to fully clustered; the weighted coefficient is much lower (0.044), indicating that the edge weights are strongly unequal despite the tight topology.

This weight disparity is the central quantitative feature of $\mathcal{B}$. Across the five percentile thresholds in Table IX, the threshold value is stable at 19.67 through the 90th percentile and then jumps to 1208 at the 95th percentile, a ratio of approximately 61 [T1]. Crossing this gap, the graph collapses abruptly: 576 of 612 edges are removed, leaving 36 edges connecting 9 active vertices, with 72 isolated vertices.

The 36-edge residue is exactly $\binom{9}{2}$: the active subgraph at the 95th-percentile threshold is the complete graph K_9, density 1.000 [T1]. We proceed to identify its vertices.

VIII. K_9 BEDROCK COLLAPSE AND PERMUTATION NULL

Having identified a K_9 as the residue of the persistent backbone at the 95th-percentile threshold, we ask which 9 spatial nodes it occupies.

A. Exact bedrock match

The 9 active nodes of $\mathcal{B}_{95}$ (the subgraph after thresholding) coincide exactly with the 9 spatial bedrock nodes of Sec. III: the 9 spatial nodes of $\mathcal{G}_7$ with degree 136. Writing the two sets explicitly from the canonical engine run,

$$\text{active nodes of } \mathcal{B}_{95} = \{6, 7, 8, 11, 12, 13, 14, 15, 16\}, \tag{10}$$

$$\text{spatial bedrock} = \{6, 7, 8, 11, 12, 13, 14, 15, 16\}, \tag{11}$$

which agree bit-for-bit [T1]. The engine-index labels depend on creation order and are not themselves meaningful; what is meaningful is that the structurally-distinguished set (universal in $\mathcal{G}_7$ and spatial) coincides with the dynamically-produced set (residue of percentile thresholding on the pair-coembedding backbone), without any tuning of either construction against the other. Figure 4 shows the thresholding visually.

TABLE X. The 9 spatial bedrock nodes identified by $\mathcal{B}_{95}$, with their full parent-overlap, shape multiplicity, and canonical shape. The shape column abbreviates $P \equiv$ primitive token; $(X|Y)$ denotes the canonical pairing of subtrees X and Y. All nine nodes have full $\mathcal{G}_7$ degree 136 (universal in the overlap graph) and DAG size 7 by definition.

local	global	p_i	m_i	canonical shape
0	6	1	2	$((((P\|P)\|P)\|((P\|P)\|P))\|P)$
1	7	1	2	$((((P\|P)\|P)\|((P\|P)\|P))\|P)$
2	8	3	1	$((((P\|P)\|P)\|((P\|P)\|P))\|(P\|P))$
3	11	3	4	$((((P\|P)\|P)\|P)\|((P\|P)\|P))$
4	12	3	4	$((((P\|P)\|P)\|P)\|((P\|P)\|P))$
5	13	3	2	$((((P\|P)\|P)\|(P\|P))\|((P\|P)\|P))$
6	14	3	4	$((((P\|P)\|P)\|P)\|((P\|P)\|P))$
7	15	3	4	$((((P\|P)\|P)\|P)\|((P\|P)\|P))$
8	16	3	2	$((((P\|P)\|P)\|(P\|P))\|((P\|P)\|P))$

Table X records the properties of these 9 nodes in the registry. Two structural observations stand out:

1. The 9 bedrock nodes are realized by exactly 4 canonical tree shape classes, with all members of each class present in the bedrock: shape A (multiplicity 2, parent overlap 1), shape B (multiplicity 1, parent overlap 3), shape C (multiplicity 4, parent overlap 3), shape D (multiplicity 2, parent overlap 3). The bedrock is thus closed under shape equivalence [T1].

2. The singleton shape class (multiplicity 1) of the DAG-7 registry — the unique asymmetric node with no canonical-form twin — lies in the bedrock [T1].

B. Weight-permutation null

To test whether the K_9 topology, the bedrock match, or both could arise by chance from the observed weight distribution on the 612 persistent edges, we run a weight-permutation null. The persistent edge set E_{pers} is held fixed. The 612 weights $\{w_{\text{pers}}(e) : e \in E_{\text{pers}}\}$ are shuffled across the edges uniformly at random. The 95th-percentile threshold is recomputed from the permuted weight vector (it equals the observed threshold exactly, since the weight multiset is preserved), the thresholded subgraph is constructed, and the following are recorded:

- n_{active}: number of nodes with nonzero degree.
- m: number of retained edges.
- ω: size of the largest clique.

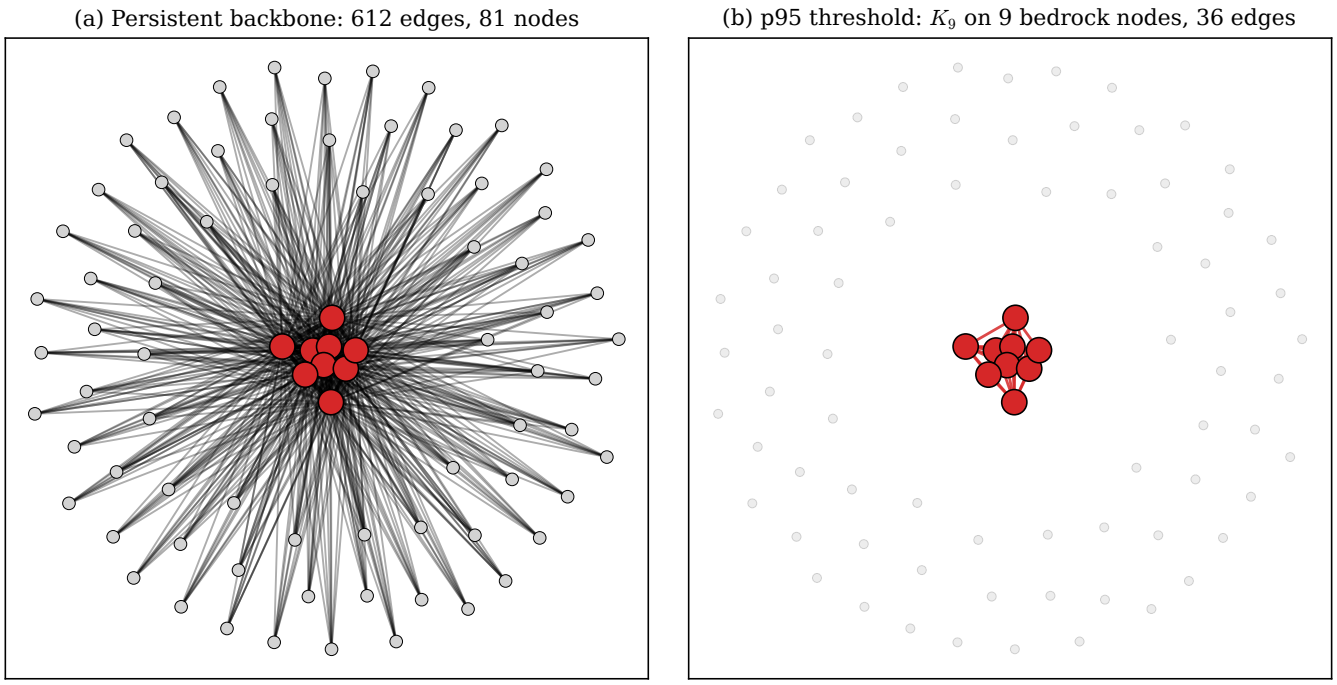

FIG. 4. The K_9 bedrock collapse. Both panels use the same node positions (weighted spring layout on the log-transformed persistent weights). (a) The full persistent backbone $\mathcal{B}$: 612 edges over 81 nodes, with edge thickness and opacity scaled by log-persistent-weight. The 9 bedrock nodes (red) sit at the visual center, pulled together by their pairwise high weights. (b) Thresholded at the 95th percentile of the weight distribution: 576 of 612 edges fall below threshold and are dropped, leaving the complete graph K_9 on the 9 bedrock nodes with 36 edges. The 72 non-bedrock nodes become isolated (shown faded). No tuning is involved: the threshold is $w = 1208$ selected automatically as the 95th percentile of the persistent weight distribution.

TABLE XI. Permutation-null results for the K_9 bedrock collapse, at $N = 10\,000$ permutations of the 612-edge persistent backbone. "Observed" is the single realized configuration from the engine. The permutation is of the weights only; the edge set is held fixed.

	observed	null (mean ± std)
active nodes n_{active}	9	36.7 ± 2.0
edges m	36	36.0
max clique ω	9	2.31 ± 0.48
Jaccard overlap J	1.000	0.243 ± 0.016
Pr(K_9 anywhere)	—	0/10 000
Pr(K_9 on bedrock)	—	0/10 000

- J: Jaccard overlap between the active-node set and the bedrock set.
- Two binary outcomes: whether the active subgraph is K_9-topology-anywhere (any 9-clique with no other edges), and whether the active subgraph matches the bedrock exactly.

With $N = 10\,000$ permutations, Table XI gives the observed probabilities.

The observed result lies outside the support of the null distribution on all three dimensions [T1]:

- In 10 000 permutations, the retained subgraph never has fewer than 29 active vertices; the observed value 9 is unreachable.
- The maximum clique under the null is ≤ 4 in all 10 000 trials (68.7% at $\omega = 2$, 31.2% at $\omega = 3$, 0.03% at $\omega = 4$); the observed value 9 is unreachable.
- The Jaccard overlap of the active set with the bedrock is 0.243 ± 0.016 under the null, essentially the expected value $9/37 \approx 0.24$ for random 9-element active sets drawn from an $\sim$ 37-element active pool intersecting a fixed 9-element bedrock; the observed value 1.000 is unreachable.

A frequentist upper bound on p for both "K_9 anywhere" and "K_9 on bedrock" is $p < 1/10\,000$ by direct count. A per-null-sample standard score for ω against the observed K_9 is $(9 - 2.31)/0.48 \approx 13.9$; the bedrock-Jaccard score is $(1.000 - 0.243)/0.016 \approx 47$. We report these as illustrative only; the count-based upper bound is the more conservative frequentist statement.

The null thus places the observed K_9 bedrock collapse far outside the range of permutation-compatible outcomes, supporting the identification of the bedrock as a structurally selected set rather than a statistical artifact of the weight distribution on E_{pers} [T1]. Figure 5

shows the null distributions graphically.

IX. CANDIDATE STEP-SPACE CLOCKS AND SCALING RATIOS

We extract from the step-space summary (Table I) four dimensionless ratios that depend only on the step index s and that characterize the growth of the engine state in different ways. The ratios are:

$$R_1(s) := \frac{\text{paths}(s)}{|V_s|} \tag{12}$$

$$R_2(s) := \frac{\text{pathDAG}(s)}{\text{paths}(s)} \tag{13}$$

$$R_3(s) := \frac{\text{regContain}(s)}{|V_s|} \tag{14}$$

$$R_4(s) := \frac{\text{regPair}(s)}{\text{regContain}(s)} \tag{15}$$

where

- $\text{paths}(s) = \sum_{v \in V_s} \text{paths}(v)$ is the total number of root-to-node directed paths in $\mathcal{P}_s$, counting every distinct route from a primitive to every object;
- $\text{pathDAG}(s) = \sum_{v \in V_s} \text{paths}(v) \cdot |\text{DAG}(v)|$ is the DAG-size-weighted path count;
- $\text{regContain}(s) = \sum_{v \in V_s} |\{R_i \in \text{DAG-7} : \text{DAG}(R_i) \subseteq \text{DAG}(v)\}|$;
- $\text{regPair}(s)$ is the number of triples (v, R_i, R_j) with $i < j$, both R_i and R_j DAG-7 registry nodes, and $\text{DAG}(R_i), \text{DAG}(R_j) \subseteq \text{DAG}(v)$.

Interpreted loosely, R_1 is the mean path count per vertex, R_2 is the path-weighted mean DAG size, R_3 is the mean number of DAG-7 sub-DAGs embedded in each object, and R_4 is the mean number of co-embedded pairs per embedded registry node. No physical claim is intended here; the four ratios are presented as candidate step-space order parameters.

A. Numerical values and step ratios

Table XII records the numerical values of $R_1, \ldots, R_4$ at each step, along with the consecutive-step ratio $R_k(s)/R_k(s-1)$.

B. Observed scaling

Three patterns in Table XII are worth recording separately:

TABLE XII. Candidate step-space clocks. "–" denotes undefined (one of the terms vanishes). Values below the step at which the registry first populates ($s = 4$) are included only where well-defined.

s	R_1	R_2	R_3	R_4
2	2.000	3.200	0	–
3	3.500	4.714	0	–
4	6.824	6.780	0.250	0
5	13.636	9.967	0.560	0.1066
6	27.272	15.193	1.104	0.3716
consecutive-step ratios $R_k(s)/R_k(s-1)$:				
3/2	1.75	1.47	–	–
4/3	1.95	1.44	–	–
5/4	2.00	1.47	2.24	–
6/5	2.00	1.52	1.97	3.49

1. The consecutive-step ratio $R_1(s)/R_1(s-1)$ converges rapidly to 2: values $1.75, 1.95, 2.00, 2.00$ at the four transitions $s = 2 \to 6$. By steps 5 and 6 the ratio is 2.000 to three decimal places [T2]. We do not claim a proof that the ratio is exactly 2 in the large-s limit; we flag this as [T2].

2. The consecutive-step ratio $R_3(s)/R_3(s-1)$ is available at only two transitions ($5/4 = 2.24$ and $6/5 = 1.97$); the apparent convergence to ~ 2 is numerically suggestive but evidence-poor, and we flag it as [OPEN].

3. The consecutive-step ratio $R_2(s)/R_2(s-1)$ is stable in a narrow band 1.44–1.52 across all four transitions. We note this numerically [T2]; a derivation of the limiting value (which we do not claim is 1.5 exactly) is [OPEN].

C. Relation to the DAG-size distribution

The ratio $R_2 = \text{pathDAG}/\text{paths}$ admits a natural interpretation: it is the mean DAG size of objects, weighted by their root-to-node path count. At step 6, the path-unweighted mean DAG size over all 2 598 062 objects is $\sum_k k \cdot n_k/|V_6| \approx 15.01$, where n_k is the count at DAG size k; the path-weighted counterpart is $R_2(6) = 15.19$, slightly larger. The two are close because the path-count distribution across objects at step 6 is mildly correlated with DAG size.

The value $R_2(6) \approx 15.19$ against a maximum DAG size of 19 and a mode of 15 at step 6 (Table II) is numerically consistent [T2]. A full analytic treatment of the DAG-size distribution and its relation to the R_k ratios is left for future work.

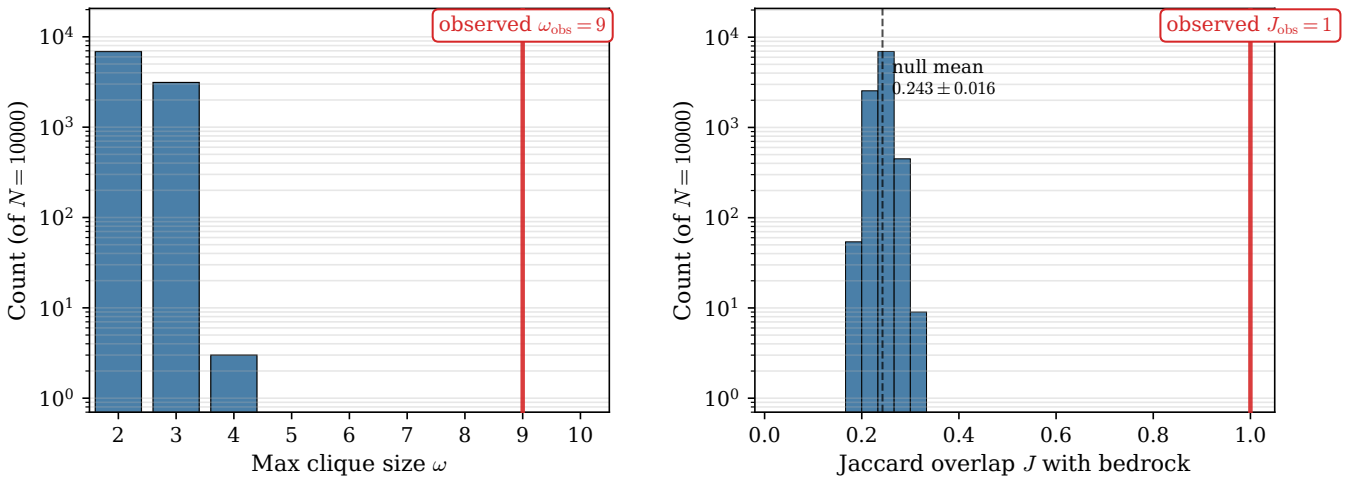

FIG. 5. Null distributions from $N = 10\,000$ weight-permutation trials on the 612-edge persistent backbone. (a) Maximum clique size ω in the 95th-percentile thresholded subgraph. The null distribution is concentrated at $\omega \in \{2, 3\}$ with a small tail at $\omega = 4$; the observed value $\omega_{obs} = 9$ is off the chart. (b) Jaccard overlap J between the active-node set and the 9-element spatial bedrock. The null distribution is a narrow peak at $J \approx 0.24$, consistent with random 9-element active subsets drawn from a $\sim$37-element active pool; the observed $J_{obs} = 1$ is unreachable. Counts use log scale.

X. DISCUSSION

The results of this paper are combinatorial. The distinction engine is defined by a single rule (two primitive tokens, unordered pairing, no self-pair), and all the numerical facts reported here follow from that rule by deterministic iteration. We have made no appeal to physical interpretation in establishing any claim at tier T1 or T2.

Prior work in the Relational Mathematical Realism (RMR) program has proposed physical interpretations for a number of the integers that now arise directly from the engine. The registry size 137, the spatial–interface–gravitational partition $(81, 40, 16)$, and the spatial bedrock size 9 are all discussed in the RMR series as structural inputs whose source was an open question [1–3]. The present paper closes that source question at the combinatorial level: these integers are produced by a minimal iterative process whose only inputs are (i) the cardinality 2 of the primitive set and (ii) the single rule that two undistinguished objects may be distinguished. The broader empirical reach of the RMR program — spanning four-force dynamics from the same 137-element registry [4], cross-scale evidence from neutron-star glitches to Compton scattering [5, 6], and cosmological observables including the CMB power spectrum and the Hubble tension [7, 8] — is covered in those separate installments and is not argued in the present paper.

Several features of the engine output have close numerical counterparts in the RMR integer set $\mathcal{A} = \{1, 2, 3, 4, 5, 9, 13, 16, 17, 40, 136, 137\}$: the 2 primitives, the overlap threshold 3, the terminal mean degree 4, the uniform tree depth 5 of the G sector, the 9 spatial bedrock nodes, the 16 G nodes, the 40 I nodes, the 136 degree of universal nodes, the 137 DAG-7 registry, and the 17 DAG-7 objects present already at step 4. The integer 13 appears as a sector edge-density denominator (the $I{-}I$ density is $419/780 = 0.537$; more transparently, $13 \times 60 = 780$). The integer 81 is not listed in $\mathcal{A}$ but is the spatial-sector size and equals 3^4. We record these numerical coincidences as observations [T1]; the physical interpretation of the correspondence is covered in the separate RMR literature and is not a claim of this paper.

Three features of the engine output we consider structurally significant in their own right, independent of physical interpretation:

1. *The uniqueness of the partition.* The joint engine+partition search over 256 configurations produces the canonical $(81, 40, 16)$ triple at exactly one point. Extensions of the search space (richer engine rules, more primitives, non-standard multiplicity cuts) are not ruled out by the present work and we flag the full-uniqueness claim as OPEN; within the tested grid, however, the result is T1.

2. *The structural signature of G.* The 16 nodes of the gravitational sector have zero variance across five independent signatures (cross-sector connectivity $(45, 21, 7)$, tree depth, leaf count, canonical shape class, multiplicity class). The interior of the high-overlap bucket is topologically homogeneous in the sense of these signatures; what isolates the 16 G nodes is not any one signature but their joint invariance.

3. *The K_9 bedrock collapse.* The coincidence of the structurally-defined bedrock (universal-in-$\mathcal{G}_7$ and spatial) with the dynamically-produced bedrock (residue of the 95th-percentile persistent backbone)

is not tuned. The two constructions are independent: the first uses only the DAG-7 overlap graph; the second uses only the layer-13-through-15 co-embedding pattern. That they produce the same 9-node set is a combinatorial fact that a permutation null of $N = 10\,000$ rules out as chance to a frequentist upper bound of $p < 1 \times 10^{-4}$.

We leave as open, for future combinatorial work independent of RMR interpretation: (a) a symbolic derivation of the $R_2(s)/R_2(s-1) \in [1.44, 1.52]$ stability band; (b) a symbolic derivation of the scaling relation between the spatial-pair concentration phase (Table VII) and the DAG-size distribution; (c) an extension of the uniqueness sweep beyond the 256-configuration grid reported here; and (d) an extension of the engine to larger primitive sets or alternative pairing rules with a view to identifying other canonical triples of sector sizes.

XI. CONCLUSION

A minimal combinatorial process on two primitive tokens, iterated under a single distinction rule, produces at step 6 a halted state of 2 598 062 objects with a DAG-size spectrum whose seventh entry is exactly 137. The 137 DAG-7 objects partition uniquely into sectors of sizes $(81, 40, 16)$ under a two-parameter partition rule, and this partition is the unique point in a 16×16 joint sweep of engine and partition hyperparameters. The 16-element gravitational sector is topologically homogeneous under five independent signatures. Embedding the registry into DAG layers 8 through 16 reveals a phased sequence of broadening, freeze-out, and concentration in pairwise co-embedding on the spatial sector; the concentration phase at layer 16 already carries the 36-edge $\binom{9}{2}$ signature. The 95th-percentile weighted backbone of the persistent spatial pair graph over layers 13–15 is exactly K_9 on the 9 spatial nodes of full $\mathcal{G}_7$ degree, matched bit-for-bit. A weight-permutation null at $N = 10\,000$ recovers neither the K_9 topology nor the bedrock identity in any single trial.

The facts listed above are combinatorial, derived from the distinction rule by deterministic iteration. Their physical interpretation within the RMR research program is addressed in separate work [1–4]; the present paper establishes only that the integers, partition, and structural signatures invoked in that program are produced by a minimal closed process, and that the process is essentially uniquely parameterized.

ACKNOWLEDGMENTS

This work was conducted independently, without institutional or external funding. Anthropic's Claude (Opus 4.7) provided assistance with code generation and manuscript preparation. All code used in this paper is available from the author upon request.

[1] J. Merwin, "Geometric origin of fundamental constants: Thirty derivations from discrete relational structure and the substrate-interface duality," viXra:2601.0081 (2026).
[2] J. Merwin, "Thermodynamic screening corrections in Relational Mathematical Realism: Mass predictions from graph topology and a universal screening unit," viXra:2603.0072 (2026).
[3] J. Merwin, "Relational Mathematical Realism: Registry architecture predicts lepton, baryon, and strange baryon mass spectra," viXra:2603.0062 (2026).
[4] J. Merwin, "Emergent four-force dynamics from a discrete 137-element registry: Gravity, electromagnetism, strong, and weak interactions via causal integer lattice simulation," viXra:2603.0003 (2026).
[5] J. Merwin, "Universal tetrahedral spacetime structure: From Compton scattering to neutron star glitches," viXra:2601.0036 (2026).
[6] J. Merwin, "Cross-scale evidence for discrete spacetime structure," viXra:2601.0070 (2026).
[7] J. Merwin, "A discrete CMB angular power spectrum from a causal integer graph: Zero free parameters, two acoustic peaks, and a convergence prediction for Planck 2018," viXra:2603.0064 (2026).
[8] J. Merwin, "Relational Mathematical Realism III: The Hubble tension as a discrete spacetime measurement artifact," viXra:2602.0116 (2026).
[9] G. Spencer-Brown, *Laws of Form* (Allen & Unwin, London, 1969).